Science and Technology Indonesia
e-ISSN:2580-4391 *p*-ISSN:2580-4405
Vol. 9, No. 4, October 2024

Research Paper

Check for updates

Detection of Dominant Rainfall Patterns in Indonesian Regions Using Empirical Orthogonal Function (EOF) and Its Relation with ENSO and IOD Events

Melly Ariska[1], Suhadi[2], Supari[3], Muhammad Irfan[4], Iskhaq Iskandar[4*]

[1]*Doctoral Student of Mathematical Sciences and Natural Sciences, Universitas Sriwijaya, Palembang, 30662, Indonesia*
[2]*Department of Physics Education, Universitas Islam Negeri Raden Fatah, Palembang, 30126, Indonesia*
[3]*Meteorology Climatology and Geophysics Agency, 3540, Indonesia*
[4]*Department of Physics, Faculty of Mathematical Sciences and Natural Sciences, Universitas Sriwijaya, Palembang, 30662, Indonesia*
***Corresponding author**: iskhaq@mipa.unsri.ac.id

Abstract
Several studies indicate that Indonesia's position on the equator, where winds from the northern and southern hemispheres converge, leads to year-round rainfall in Indonesia. Previous studies have also shown the presence of monsoon winds over Indonesia, which causes rain in Indonesia to follow the Asian and Australian monsoon wind patterns. Recently, variations in rainfall patterns and intensity in Indonesia have been highly volatile and difficult to predict. This study uses gridded data analysis of ocean-atmospheric rainfall for 69 years (1948–2016) to detect monsoonal, equatorial, and local signals and relate them to ENSO and IOD events. Rainfall analysis reveals that the first mode accounts for 38.57%, the second 13.92%, and the third 8.93% of the total variance. These results show that these variants are very variable, both in space and time. Monsoonal patterns were detected in the southern region of Indonesia, equatorial patterns in northern Sumatra and western Kalimantan, while local patterns were detected in Maluku and the Maluku Islands. Furthermore, the monsoonal and local rainfall patterns are strongly correlated (> 0.85) with local SST, but the equatorial rainfall pattern is weakly correlated (< 0.5) with local SST. Note that the equatorial pattern is associated with the Inter-Tropical Convergence Zone (ITCZ) phase. The varied vector correlation map illustrates the asymmetric fluctuations in sea surface temperature and the simultaneous existence of winds coming from the west from the Indian Ocean and winds coming from the east from the Pacific Ocean during the period of heavy precipitation.

Keywords
EOF, ITCZ, Monsoonal Winds, Rainfall Variability, Sea Surface Temperature

Received: 25 June 2024, Accepted: 29 September 2024
https://doi.org/10.26554/sti.2024.9.4.1009-1023

1. INTRODUCTION

The monsoon and the convergence zone's northward and southward displacement in response to the sun's visible shift are related to Indonesia's precipitation (Kajita et al., 2022). When two circulations of air from different poles of the atmosphere collide, the air rises to the integration zone. Convergence is a shift of wind to a point that results in upward movement, and the area where integration arises is known as a converged area. (Yamanaka, 2018). The Inter-tropical Convergence Zone (ITCZ) is a very limited region that occurs at low latitudes. The ITCZ is also known as the heat equator or equatorial front (Lestari et al., 2019; Liu et al., 2024). The position of the Atlantic and Pacific Oceans of the ITCZ is very closely connected to the doldrums (5°N-5°S area), so the ITCZ is the boundary between the strong maritime airflow from the northeast to the southeast, while over the continent the shift in the ITCZ position appears more pronounced. The monsoon circulation is connected to the north-south shift of the ITCZ and also depends on seasonal contrasts in land and ocean heating as a complex system (Nugroho et al., 2021). The ITCZ moves northward in boreal (northern hemisphere) summer (July) and moves southward in boreal winter (January) following the location of maximum solar heating. In July, when the summer maximum occurs in the Northern Hemisphere, the position of the ITCZ is around 25° N above the Asian continent and between 5 and 10° N above the ocean (Ariska et al., 2024a; Zhang et al., 2020; Zheng, 2019). In January, when the summer maximum occurs in the Southern Hemisphere, the ITCZ is around 15° S above the land (continent) and near the equator above the ocean. The ITCZ's position will definitely have an impact on rainfall in areas where it has been detected, and this will probably result in wet periods and rainy weather. Twice a year, the ITCZ occurs exactly on the equator, namely in

September and March. Therefore, in these months above the equator there is a convergence that contributes to increased rainfall (Iskandar et al., 2022).

Many studies show the existence of monsoon winds in Indonesia (Liu et al., 2024; Mulsandi et al., 2024). However, Because of research indicating that the region close to the equator between 10°S and 10°N does not fit under the conventional monsoon climate because it receives abundant annual rainfall, this region is still not properly characterized. (Campos et al., 2024; Estrela et al., 2024). Indonesia is understood as an island on the equator, which is marked by two times the annual maximum amount of rainfall and a protracted rainy season that is followed by a brief dry season. For regions south and southeast of the equator, the dry season will progressively lengthen (Ariska et al., 2024b). A monthly rainfall pattern having 2 (two) maxima within a year is known as a bimodal pattern. The study of regional monsoons, many scientists would like to focus on other massive quantities phenomena, such El Nino–Southern Oscillation (ENSO), rather than discussing how these monsoon and equatorial regions are detected. The Meteorology, Climatology, and Geophysics Agency is still working at tracking Indonesia's rainy season activity using the AUSMI index, which is based on local rainfall in Australia (Chang et al., 2005; Liu et al., 2024; Zhang et al., 2020), while the monsoon is a strong regional characteristic (Liu et al., 2024; Mulsandi et al., 2024). Thus, in an attempt to reduce the detrimental effects of hydrometeorological disasters on the environment and economy in these regions, it is imperative to first define the area of Indonesia's monsoon, equatorial, and local rainfall patterns.

The link between SST and rainfall patterns over the Indonesian region has been demonstrated by earlier investigations (Aldrian and Susanto, 2003; Ariska et al., 2024a,b; Mulsandi et al., 2024). They demonstrate how suppression of (increased) evaporation in response to cooling (warming) leads to decreased (higher) rainfall. Additionally, the variability of rainfall in Indonesia may be considerably influenced by both local and distant SST. The simultaneous influence of both nearby and far-off SSTs, however, makes it challenging to identify which has the greatest impact on Indonesia's rainfall variability. This emphasizes the need for a deeper comprehension of the dynamics behind Indonesia's rainfall variation. Furthermore, the majority of earlier research relied on straight forward analytic techniques like composites and correlations based on certain reference grid points or indices, which necessitate subjective interpretation of the time series selection. Thus, the EOF approach is used in this work to investigate the temporal evolution, spatial pattern, and interaction of rainfall variability with SST and the patterns of winds.

In order to analyze spatial forms of variability and their temporal variations, EOF analysis has been applied extensively. There is no physical foundation for the EOF analysis. It is accomplished by computing the eigenvalues and eigenvectors of an anomalous covariance matrix of a set of data that is weighted geographically. The fraction of variation that each mode explains is represented by the computed eigenvalues. The time series of the different modes (principal components) are created by projecting the resulting eigenvectors onto the spatially weighted anomalies. The amplitude of each mode across the data period will be the outcome (Iskandar et al., 2022; Lestari et al., 2019; Mulsandi et al., 2024). Furthermore, the precipitation data that was used, which was derived from climatic data products from the Princeton Global Meteorological Forcing Dataset, had a large time span and high resolution, spanning from January 1948 to December 2016. This data has daily spatial resolution and high spatial resolution (0.250 0.250). This enables more in-depth study at the regional and global levels. This data, which includes regions with little direct observational data, like the oceans and remote locations, is created by combining observational data and reanalysis models covering the whole surface of the world. Princeton University's monthly rainfall data has been used in a number of research, such as those by Zhang et al. (2020) and Beck et al. (2017).

This study attempts to determine the temporal and spatial variations of rainfall in Indonesia and connect it to ENSO and IOD. For this purpose, we first performed an EOF analysis to detect monsoonal, equatorial, and local rainfall signals. These three signals are, then, classified based on their spatial characteristics. Second, we conducted correlation analysis between SST and wind on precipitation to explain possible influences of tropical climate modes.

2. EXPERIMENTAL SECTION

2.1 Data Collection

This research examines monthly rainfall data over the Indonesian region, bound by an area between 11° S to 6° N and 90° to 140° E, as shown in Figure 1. Monthly precipitation data from Princeton University in link `http://hydrology.princeton.edu/data/pgf/v3/0.25deg/daily/` (accessed on 14 April 2023) is used to create monthly rainfall data with a horizontal resolution of 0.250 0.250 is taken from monthly precipitation data from Princeton University. This study employs monthly SST, vertical velocity, zonal wind (u10), meridional wind (v10), and rainfall data from the ERA5 monthly averaged data link `https://cds.climate.copernicus.eu/` (accessed on 8 November 2023). National Center for Environmental Prediction (NCEP) is an advanced version of the NCEP-NCAR reanalysis. The selection of this study area is expected to represent the response to the impact of precipitation variability, especially precipitation in the Indonesian region. The mean precipitation in each region of Indonesia calculated from 1948-2016 can be seen in Figure 1.

2.2 Methods

2.2.1 EOF Analysis

The EOF technique looks for a new set of variables that represent most of the observed variance in the data by utilizing a linear combination of the original variables. Since the early 1950s, atmospheric scientists have developed Empirical Orthogonal Functions (EOFs), as demonstrated by the works of Obukhov (1947), Obukhov (1960), Fukuoka (1951), and Lorenz (1956).

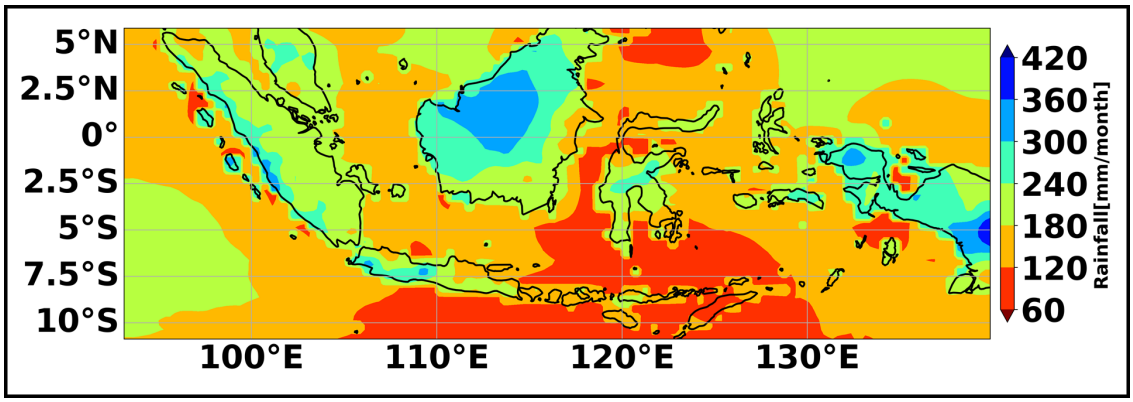

Figure 1. Average of Rainfall for Each Region of Indonesia

Lorenz (1956) invented the EOF terminology and used it in a Massachusetts Institute of Technology forecasting study. EOFs have now widely used as analysis tools in the field of climate research.

A matrix is broken down into three parts by EOF: a diagonal matrix with single values along its major diagonal, two orthogonal matrices (sometimes referred to as the left and right single vectors), and a matrix. In this work, EOF is employed to examine the spatiotemporal variability of climatic modes, identify their patterns, and further measure the significance of each pattern. Spatial and temporal modes are meant to be kept apart via EOF. Our research focuses mostly on data variability analysis instead than long-term trends. EOF analysis is a statistical technique that reduces data by constructing a new coordinate system with maximum variance by changing a previous linear system of coordinates. Data dimensions can be decreased via principal component analysis without materially altering the data's qualities. In technical terms, EOF analysis is a method for taking large amounts of multivariate data and reducing them so that an initial or original data matrix can be changed (transformed) into a smaller set of linear combinations that nevertheless capture the majority of the variation from the original data. The explanation of as much variance in the original data with as few principal components as possible is the primary objective of EOF analysis.

In addition, The EOF is a technique for identifying recurrent patterns that are changing over time and space based on data (Tang et al., 2024). Reducing a high number of data variables to a small number of variables while maintaining the majority of the original data's variation is the primary goal of EOF analysis (Horii et al., 2022; Lestari et al., 2019). The Indonesian Region's spatial and temporal patterns can be found using the EOF approach, which is expected to extract information directly from the rainfall data so as to classify the spatial and temporal ocean-atmosphere phenomena recorded in the data. Finding the covariance matrix from the rainfall data matrix is the first step in the EOF analysis process which has been defined in Equation (1), namely (Iskandar et al., 2008, 2017):

$$\Sigma = \frac{1}{n-1} X^T X \tag{1}$$

The covariance matrix Σ in Equation (1) is a real symmetric matrix that has eigenvectors $e_m(x, y)$ and positive eigenvalues λ_m. By using eigen values equation, the eigen values can be written as in Equation (2):

$$RE_m = \lambda_m e_m \tag{2}$$

From Equation (2), the eigenvalue λ and the eigenvector e are obtained which satisfy the equations $|R - \lambda 1| = 0$ and $(R - \lambda 1)e = 0$. The eigenvector is an orthogonal EOF temporal variability, thus satisfying the Equation (3) (Lyons, 1982):

$$\Sigma_{x,y=1}^{N} e_m(x_i, y_i) e_n(x_i, y_i) = 0, m \neq n \tag{3}$$

Forecasting the original data on the temporal variability yields the new equation, which is the spatial variability $u_m(t)$. Singleton defines it as the multiplication of the eigenvector $u_m(x, y)$ with the initial data matrix $X(s, t)$ which is defined in Equation (4):

$$u_m(t) = \Sigma_{x,y=1}^{N} X(x, y, t) e_m(x, y) \tag{4}$$

2.2.2 Correlation Map

Based on the recommendations of Iskandar et al. (2022) and Aldrian and Susanto (2003), we investigated the statistical results of EOF analysis using homogeneous and heterogeneous correlation maps. Vector representing the relationship between eigen value at each grid point and its h-th mode expansion coefficient. This indicator allows for the efficient evaluation of the geographical distribution of the current covariance components and their h-th modes. In order to build a correlation between two planes, the h-th heterogeneous correlation map is defined as an array of correlation values that depicts the relationship between the grid points of one plane and the expansion coefficients of the h-th mode of that plane. In order to build a correlation between two planes, the h-th heterogeneous

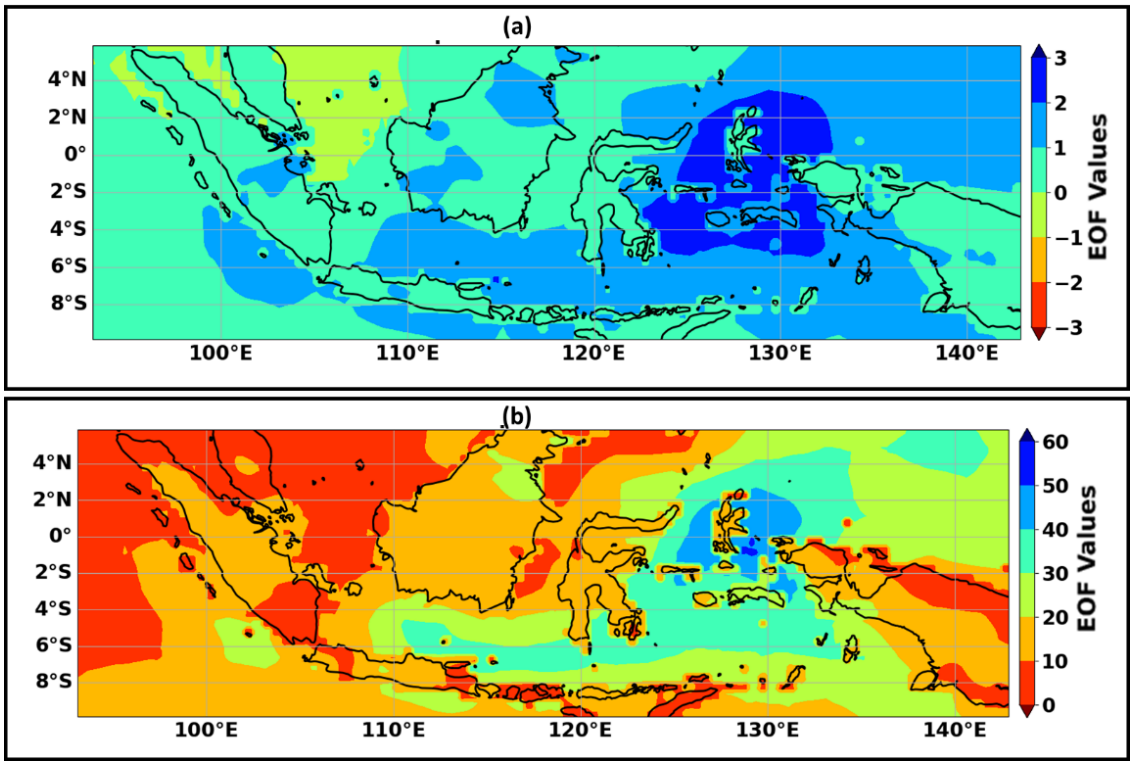

Figure 2. Spatial Mean (a) and Standard Deviation (b) at EOF1

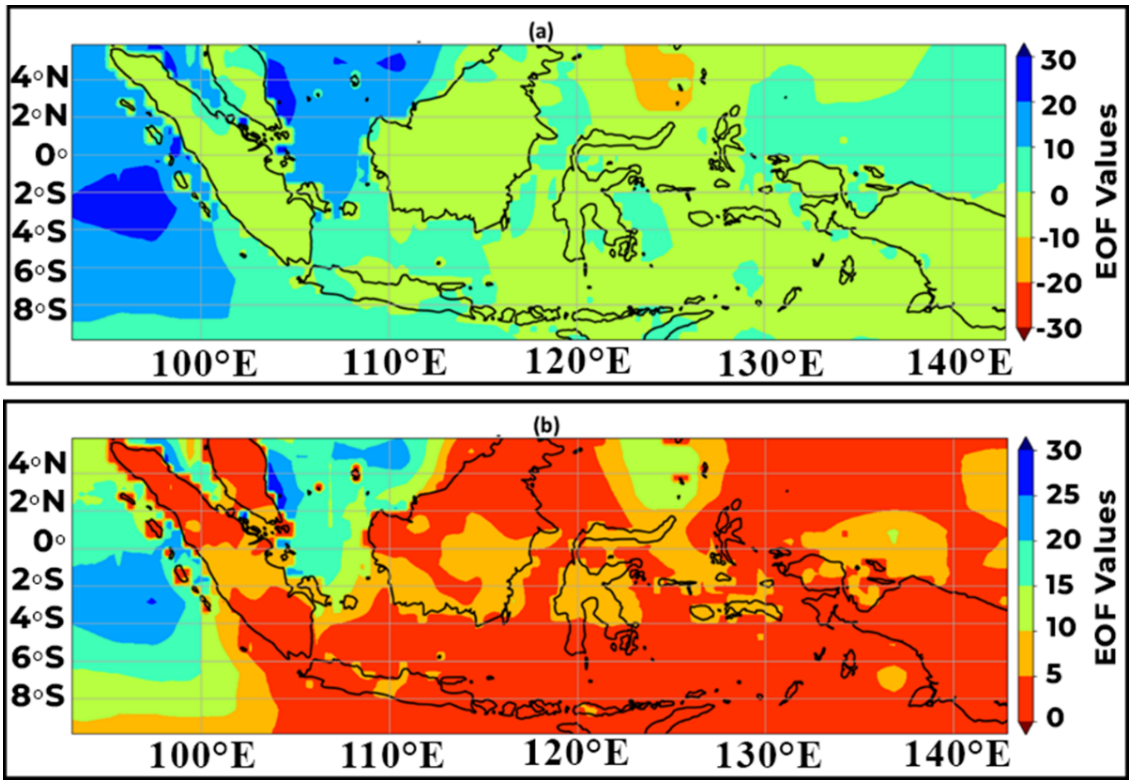

Figure 3. Spatial Mean (a) and Standard Deviation (b) at EOF2

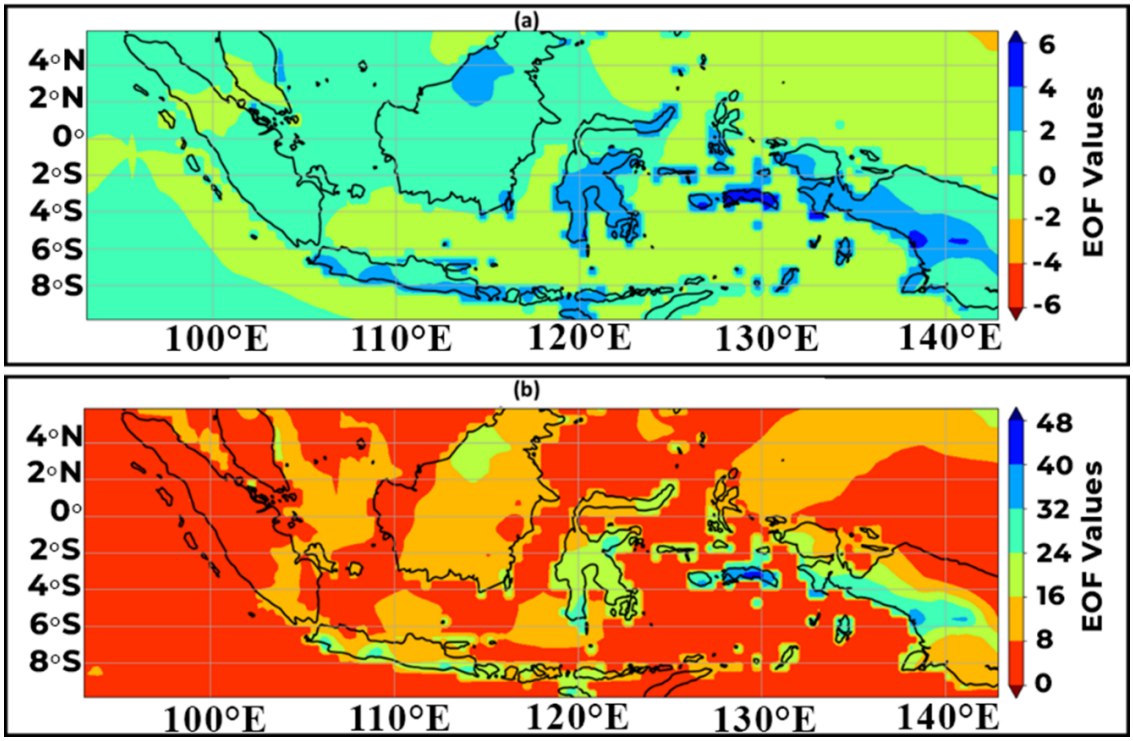

Figure 4. Spatial Mean (a) and Standard Deviation (b) at EOF3

correlation map is defined as an array of correlation values that depicts the relationship between the grid points of one plane and the expansion coefficients of the h-th mode of that plane. This statement explains how far it is possible to forecast with certainty the values of the grid points in the second plane.

When using EOF, the relationship between a particular variable's h-th expansion coefficient and the matching grid of point values is represented by the correlation map for the h-th mode. Homogeneous map would show correlation between the same variables, but a heterogeneous map would show correlation between different variables included in the EOF. In every instance, the contours that are shown show the distribution of the current modes of action centers, scaled as correlation coefficients. The process of creating vector correlation maps involves figuring out how well the h expansion coefficients of one variable correlate with different vector field elements, like the and components of the wind vector. The obtained correlation values can be characterized as vector correlation components. The strength of the association is directly proportional to the length of the arrow, which represents the direction of the wind.

2.2.3 Fast Fourier Transform (FFT) Spectrum Algorithm

Cooley et al. (1969) created the Fast Fourier Transform (FFT) analysis method. The Discrete Fourier Transform (DFT), a technique for evaluating signals or data in the frequency domain, is sped up by this algorithm. In order to identify the dominant frequency of the corresponding PC, rainfall anomalies with the highest power/amplitude in the time series are analyzed using FFT. When determining a sequence's DFT, this algorithm is crucial. Time signals can be transformed into frequency domain signals using FFT. When DFT is used for periodic spectral analysis of signals, it displays mathematical properties that are strikingly comparable to those of the integral Fourier transform. For a series with N terms, the FFT approach only needs $2NLog2N$ operations, whereas the DFT approach takes N squared (N^2) operations. As a result, the FFT method quickly and accurately produces spectral data and accelerates the harmonic analysis process. Since DFT and the Fourier transform of continuous waveforms are closely related, DFT is frequently substituted with FFT Yamanaka (2016).

DFT exhibits mathematical characteristics in the periodic spectral analysis of signals that are very similar to the integral Fourier transform. The DFT approach for a series with N terms require N squared (N^2) operations, while the FFT only requires $2Nlog2N$ Thus, the FFT technique efficiently generates spectral data and performs harmonic analysis with increased speed while maintaining high accuracy. DFT is strongly connected to the Fourier transform of continuous waveforms, i.e., FFT is often used instead of DFT Yamanaka (2016).

The FFT algorithm's representation of the rainfall time series as a function of $\gamma(x, y, t)$ is presented in Equation (5), where x is the number of pixels or longitude, y is the number of lines or latitude, and t is the time measured in months. Therefore, $\gamma(x, y, t)$ can be written as a linear combination of elementary periodic functions as in Equation (5):

$$\gamma(x, y, t) = \Sigma_{(}^{n} m = 1) A(x, y)_n e^{i[(\omega nt - \phi(x,y))_n]} \quad (5)$$

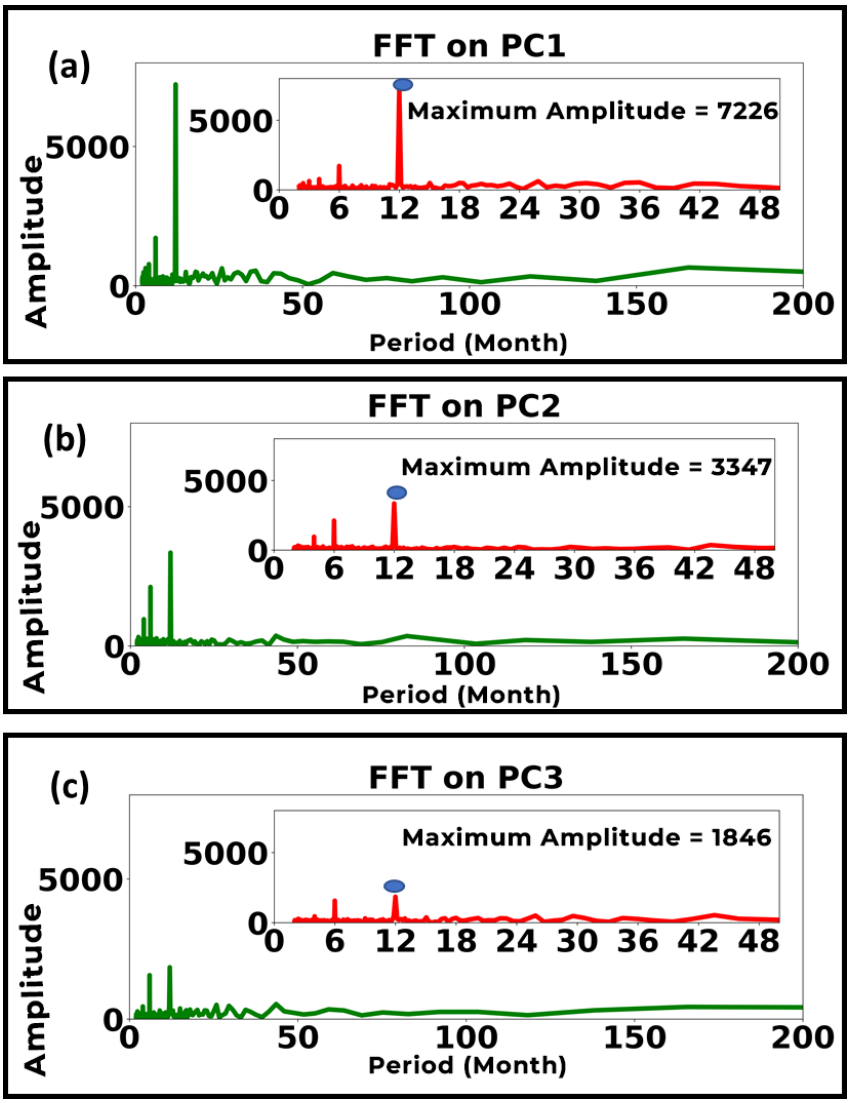

Figure 5. Spatial Mean (a) and Standard Deviation (b) at EOF3

where ω_n is the frequency, A is the amplitude, and g is the phase lag. The frequency is directly proportional to the period τ with $\omega_n = 2\phi/\tau_n$. Φ represents a collective series of events that occur within a cycle. The phenomenon is a specific time span that is defined by a particular combination of amplitude and phase that repeats a sequence of phenomena.

2.2.4 Composite Analysis

We used composite analysis as suggested by Ge et al. (2024) and Katsumata et al. (2018). Composite analysis is used to understand rainfall patterns over a certain period of time by combining data from various sources or periods. By implementing the combined or average value of the primary PC, SST, zonal wind (u10), and meridional wind (v10) at 10 meters above sea level, the spatial influence of each climatic mode event (i.e., IOD and ENSO) on rainfall in Indonesia is computed and observed. In the years when Indonesia had IOD (positive and negative IOD) and ENSO (El Nino and La Nina) events, this average is computed using the composite approach. Compared to the SST anomaly covering the southeastern portion of the tropical Indian Ocean and the Indonesian Sea, the SST anomaly covering the equatorial region of the western Indian Ocean and the eastern equatorial Pacific Ocean is colder. In Indonesia, the SST anomaly during negative IOD is warmer than that during the La Nina event. The maximum intensity of positive SST anomalies in this region is +1.0°C under negative IOD phenomenon. In the meantime, the greatest intensity during La Nina is approximately +0.7°C. Increased water vapor in the lower atmosphere as a result of wind convergence brought on by the warm SST anomaly increases atmospheric convection activity over the maritime continent. In Indonesia, the result of this scenario is an increase in rainfall.

On the opposite side, Indonesia's climate is significantly impacted when ENSO occurrences take place during the ASO

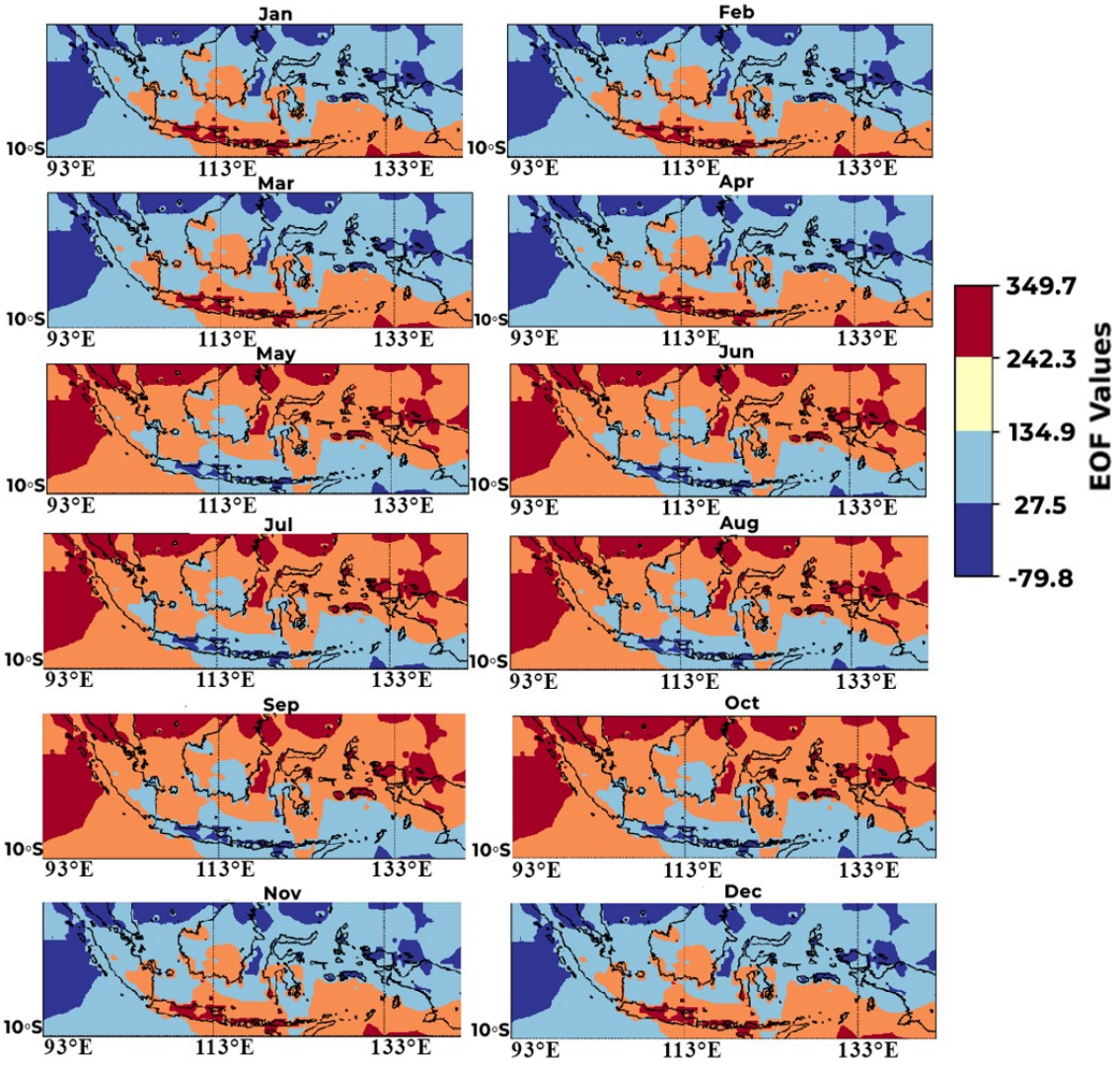

Figure 6. Monthly Climatology EOF1 from January 1948 to December 2016

and NDJ seasons. Rainfall and the ENSO and IOD climate mode indexes form a related pattern during the ASO and NDJ seasons. The classification of dry years caused by the El Nino event was obtained based on the analysis of SST anomalies in the Nino3.4 region and the gradients of the West Tropical Indian Ocean and Southeast Tropical Indian Ocean, namely in 1951, 1957, 1963, 1965, 1967, 1969, 1972, 1976, 1982, 1986, 1987, 1991, 1994, 1997, 2002, 2004, 2006, 2009, and 2015. Positive IOD years were found in ten out of the nineteen drought years. Conversely, rainy years, which happened in 1949, 1950, 1954, 1955, 1964, 1971, 1973, 1975, 1988, 1998, 2000, 2010, 2016, are normalized rainfall anomalies above 1.0. Eleven positive IOD events that coincided with El Nino events are considered to be part of the IOD phenomena, whereas three non-El Nino/La Nina years and nineteen La Nina years included eight negative IOD events.

3. RESULTS AND DISCUSSION

3.1 Detection of Dominant Rainfall Patterns in Indonesia

The variance of the ten primary modes obtained from the EOF analysis of rainfall data from Indonesia is shown in Table 1. The percentage of this fraction to the overall variation is provided. Principal components (PC) are a spatial pattern that symbolizes the explained variance for each mode. The PC time series is the temporal evolution of the PC pattern. The results of the computations indicate that there are multiple forms of rainfall variability in the Indonesian area.

Based on the multiple correlation method (DCM), Aldrian and Susanto (2003) identified the monsoon area, which is similar to the distribution of areas seen in PC1. But we did notice a little change in the areas of Kalimantan and Sumatra. As a result, utilizing a fresh dataset, the results offer an updated representation of the PC1 region. The increased spatial load on the variance—nearly three times higher than the other

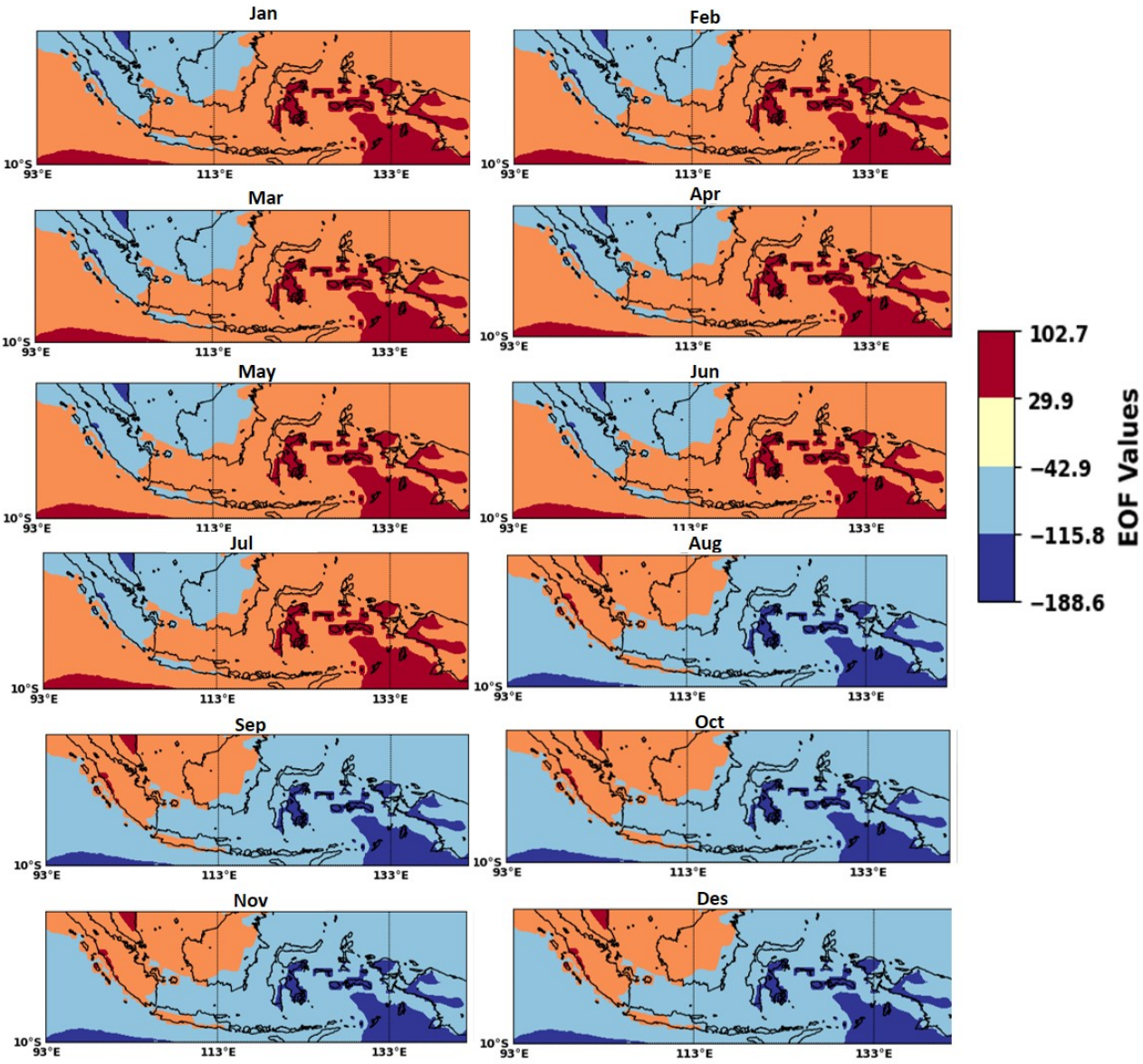

Figure 7. Monthly Climatology EOF2 from January 1948 to December 2016

modes—indicates that the first PC (Figure 2) has the strongest dominant pattern in southern Indonesia. The network in the southern and northern regions of Indonesia clearly differs from one another, indicating that the northern region of Indonesia has comparatively modest loading. Identified geographical the monsoon pattern shown in the PC pattern is somewhat reminiscent of the winter monsoon pattern seen in Asia. Consequently, this disproves the assertion that and clarifies the presence of the Indonesian monsoon (Baeda et al., 2019; Hendon, 2003; Kurniawati et al., 2020).

The second PC (Figure 3) has the second dominant pattern in Indonesia, which was detected in the western part of Sumatra Island and the western part of Kalimantan Island. This is indicated by the higher spatial load on the variance, almost three times greater than other modes. Geographically, the observed PC pattern shows an equatorial pattern because it coincides with the equator in Indonesia. Meanwhile, the third dominant pattern was detected in Maluku and the Maluku Islands, as shown in Figure 4.

In order to identify the emergence of these three signals, we utilized the FFT method to examine the frequency of PC time series. Figure 5 illustrates an examination of the Indonesian rainfall temporal pattern using PC1, PC2, and PC3 modes. There are six months in the dry phase and another six months in the wet phase, as indicated by the significant spectral peak seen in the PC1 power spectrum linked to rainfall anomalies for the time series FFT power spectrum's one-year frequency range (see Figure 5). Based on FFT analysis of the periodicity of each

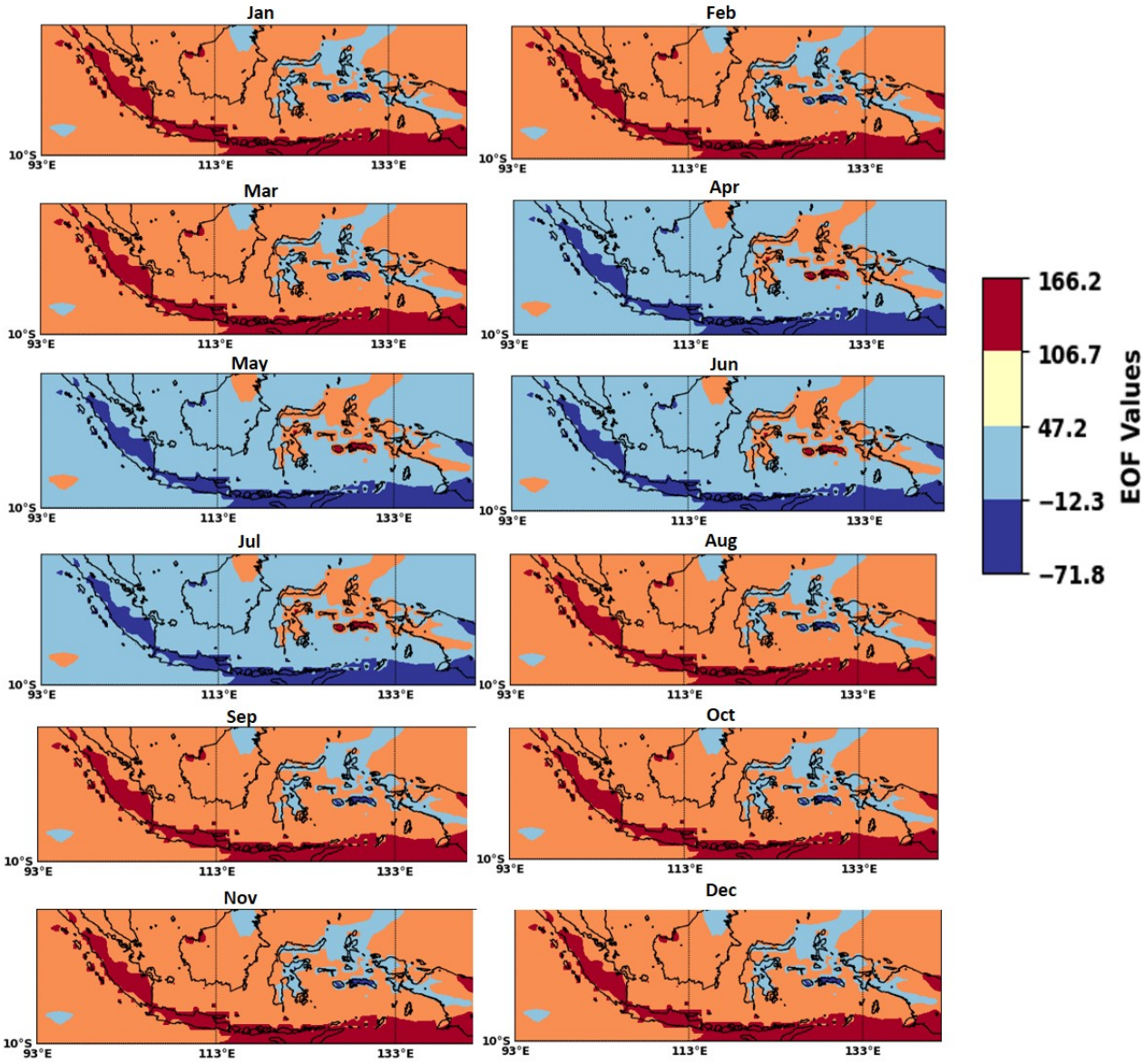

Figure 8. Monthly Climatology EOF3 from January 1948 to December 2016

PC time series produced using EOF analysis, the remaining PCs depict non-annual patterns (Aldrian and Susanto, 2003; Iskandar et al., 2017).

The periodogram of each PC is investigated to clarify which frequencies dominate the rainfall pattern in each region from each main coefficient of the resulting EOF mode. Figure 5 shows the eigenvalue spectrum of the three main regions of the resulting EOF. Along the x-axis are displayed significant time scales, which has annual (12-monthly) signals. The spectrum of the EOF1 region has a strong annual signal with amplitude values of 7226, 3347, and 1846, respectively. Minimum standard deviation of the annually cycle further suggests a strong homogenous pattern in the significant seasonal signal of the EOF1, EOF2, and EOF3. In addition, there are signals that appear over a period of more than a decade that may be related to the Indo-Pacific mode.

The results of the monthly climatological average PC values for the three main EOF regions show different climate patterns. The rainfall pattern detected in the PC1 region is the opposite of PC3, which can be observed in Figure 6-8. The finding is consistent with earlier studies' findings, including those of Aldrian and Susanto (2003), which were discussed in the preceding sub-chapter. Meanwhile, the EOF2 region has different fluctuations from the other two regions.

The EOF spectrum highlights a strong annually (12-monthly) signal, as seen in Figure 5. The monsoon, equatorial, and local signals based on the rainfall cycle that appears on the PC can be identified using the findings of the EOF analysis that has been

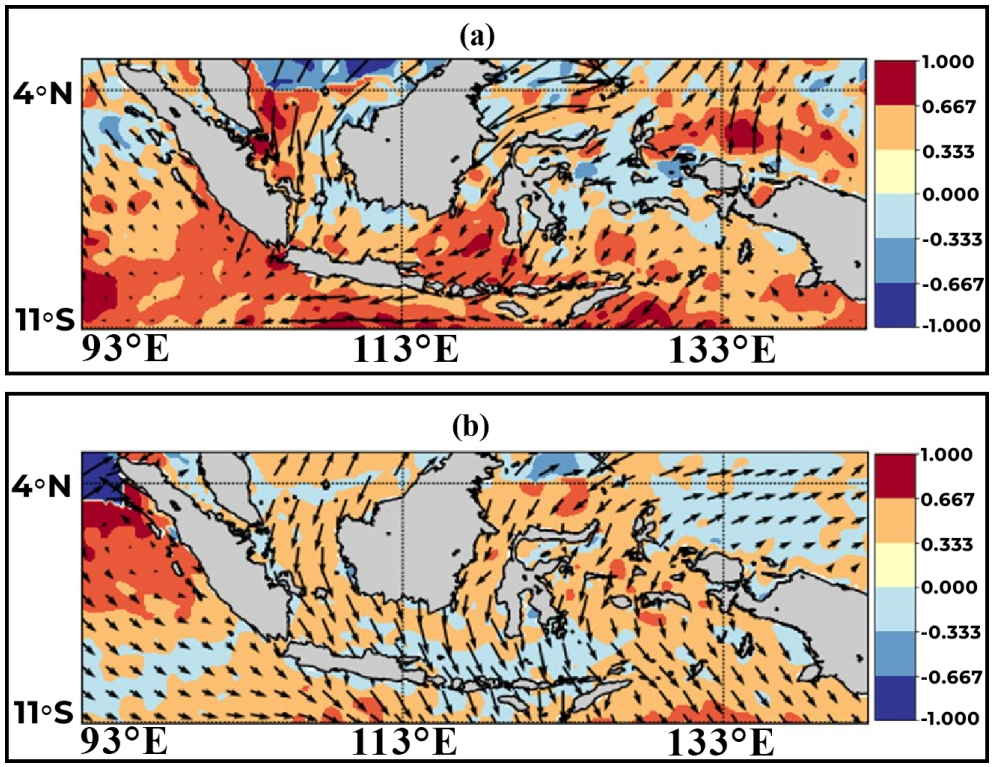

Figure 9. Correlation of SST, Zonal and Meridional Wind on EOF1 (a) ASO and (b) NDJ

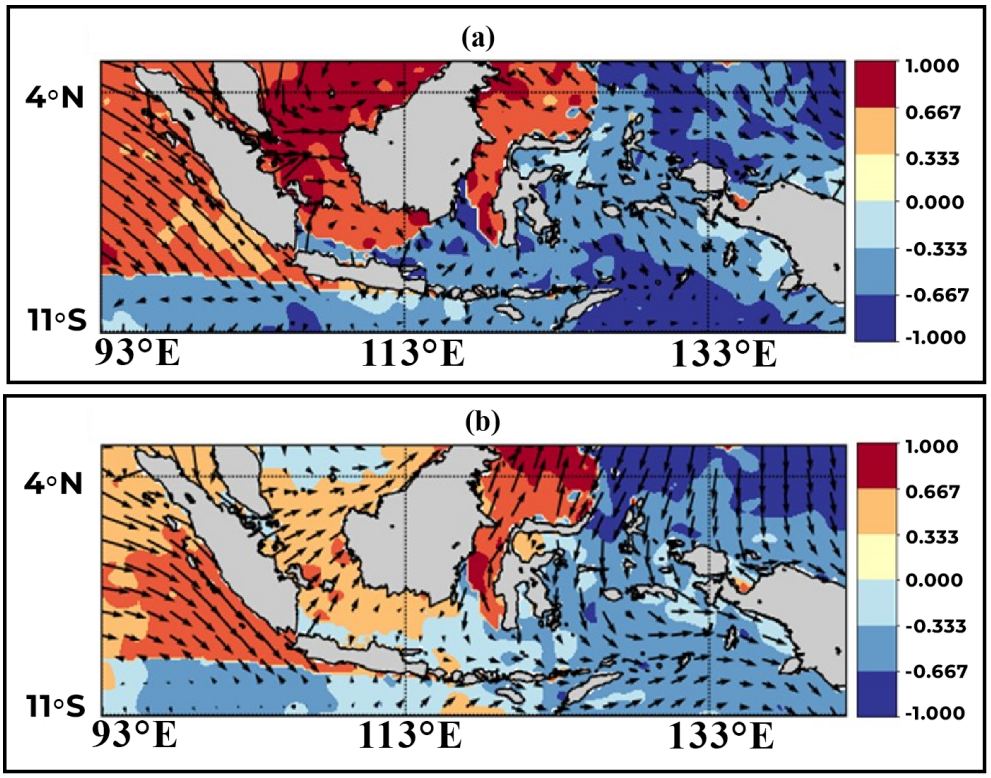

Figure 10. Correlation of SST, Zonal and Meridional Wind on EOF2 (a) ASO and (b) NDJ

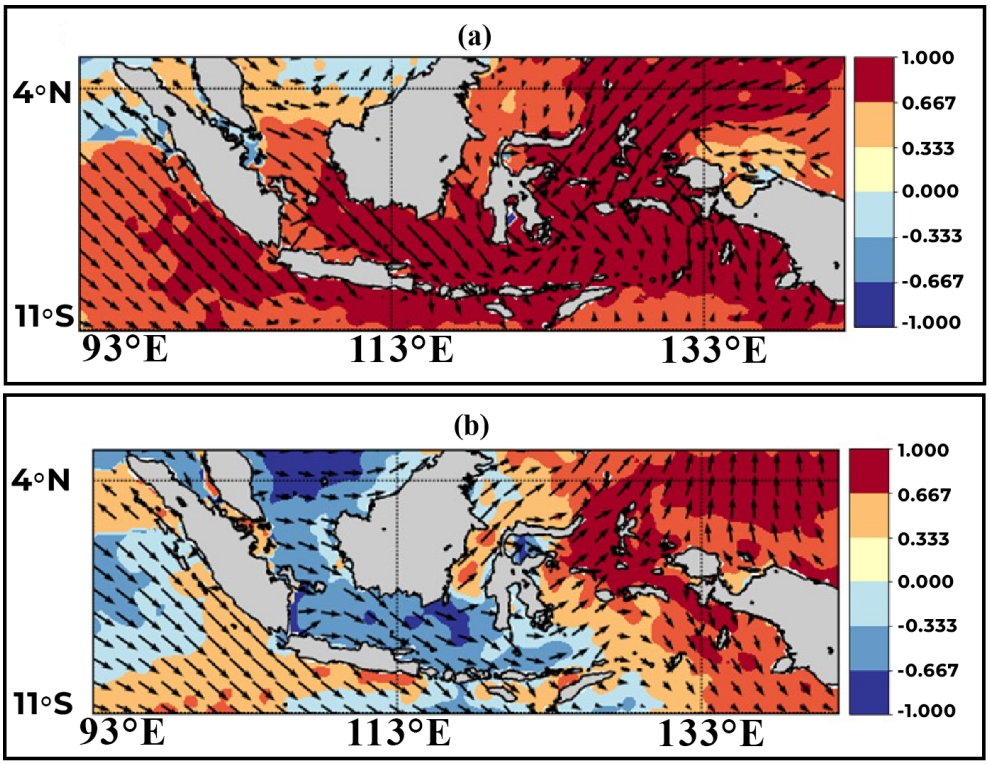

Figure 11. Correlation of SST, Zonal and Meridional Wind on EOF3 (a) ASO and (b) NDJ

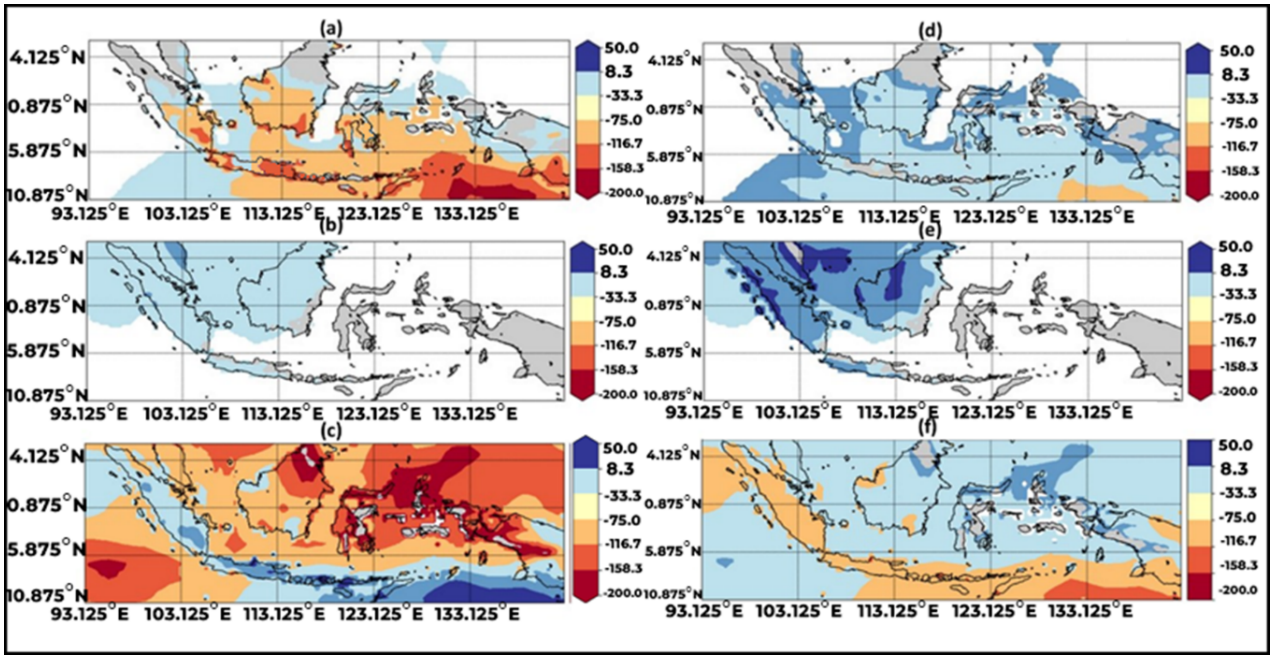

Figure 12. Composite EOF in the Neutral Year for (a) (d) EOF1, (b) (e) EOF2, and (c) (f) EOF3 for the ASO (left) and NDJ (right) Seasons. The Two-tailed t-test's 95% Significant Rainfall Anomalies Are Indicated by Color

conducted. The EOF technique yields distinct boundaries and demonstrates that annual signals and a few semi-annual signals predominate in the spectrum.

3.2 Simultaneous Correlation of Dominant Patterns with SST and Wind

In order to improve comprehension of the impact of SST and wind on dominant rainfall patterns, correlation analysis is

Table 1. Percentage of Variance of Ten PCs of Rainfall Variability in Indonesia Using EOF Analysis

PCs	Eigen Values	
	Variance	Cumulative
PC1	38.57%	38.57%
PC2	13.92%	52.50%
PC3	8.93%	61.40%
PC4	5.74%	67.17%
PC5	3.16%	70.34%
PC6	2.33%	72.68%
PC7	2.09%	74.77%
PC8	1.72%	76.50%
PC9	1.43%	77.93%
PC10	1.39%	79.33%

applied between the primary PCs and relevant atmospheric dynamic variables (wind and SST). The data indicate a strong (r = 0.86) correlation between the precipitation and local SST first PC time series. Figure 9-11 illustrates the correlation coefficients for PC2 and PC3, which are 0.78 and 0.68, respectively.

These results illustrate the correlation of EOF1, EOF2, and EOF3 providing results that are in line with the previous analysis. In Indonesia, the ASO and NDJ periods, which mark the closing of the dry season and the opening of the rainy season, have a positive correlation between local SST and EOF1, EOF2, and EOF3. This correlation explains that warm local SST increases the convective zone around Indonesian waters, both at PC1, PC2, and PC3, thereby influencing the intensity of rainfall in the region.

The primary consistent PC map relating to variations in sea surface temperature (SST) and rainfall during the Indonesian monsoon is shown in Figures 7-9. Strong positive SST loading in surrounding Indonesian waters defines the spatial pattern of the first dominant phase. A dipole pattern of rainfall with negative (positive) changes in the north (south) accompanies this variability. This demonstrates that rainfall is increased in the southern part of Indonesia during the positive phase of the local SST, particularly in locations where the correlation coefficient is large. The Java Sea, South Java Sea, Timor Sea, Arafura Sea, Flores Sea, and Banda Sea have the biggest yearly SST cycles, as seen by Figure 7, where the pattern demonstrates larger loading concentrations in comparison to the surrounding climate. These findings are consistent with earlier research (Baeda et al., 2019; Chang et al., 2004; Igarashi and Suryadarma, 2023) that demonstrates a robust relationship between rainfall in region A (monsoon region) and the local SST of South Maluku or the Timor Sea (15–5° S, 120–135° E) (Aldrian and Susanto, 2003).

This is significant evidence of the Asian winter monsoon's dominant influence on Indonesian SST variations, as previously reported by Chang et al. (2004) and Iskandar et al. (2022). It also shows that rainfall and SST variability in Indonesia are clearly influenced by monsoon activity. Large regions south of 5° S are cool (warm) during the southeast monsoon, which runs from June to August (December to February). To identify the primary dynamic driving forces of the dominant mode, more investigation is done. Thus, using the 850 hPa wind regression and each main component (PC) as a guide, we generate SST correlation maps. The lowest point of air circulation at this wind speed was selected since there are no surface disturbances at this wind velocity (Annamalai et al., 2010). It is becoming increasingly evident that the SST response to changes in air circulation brought on by local warming of Indonesian SST is linked to predominant rainfall variability. Convection, which is dependent on SST, is the predominant atmospheric mechanism, and as a result, the SST and atmospheric dynamics of the Indonesian region have a significant impact on the status of the atmosphere in the region. An overview of Indonesia's predominant rainfall coverability, as well as that of the atmosphere and oceans, has been given. This work aims to give an overview of climate predictability, since local agriculture is greatly impacted by rainfall variability in a given region.

3.3 The impact of ENSO and IOD on Indonesia's Predominant Patterns of Rainfall

The mean precipitation in the three primary EOF mode zones (non-El Nino/La Nina, positive and negative IOD) in neutral years. Figure 12 demonstrates how EOF1, EOF2, and EOF3 all clearly display the decrease in rainfall that occurs during the ASO season. Rainfall in EOF3, however, is extremely infrequent and uneven when compared to a neutral year's equivalent. Figure 12 also illustrates how precipitation in these three places is significantly decreased near the end of the dry season in the ASO season during neutral years.

During the ASO season, there is little to no rainfall, particularly in the EOF3 region, where there is very little rainfall. Meanwhile, during Indonesia's NDJ season, there is heavy rainfall virtually year-round in every location. In particular, when calculating rainfall on an annual average basis, the EOF2 region experiences more rainfall than the other two modes.

The composite results of EOF1, EOF2, and EOF3 reconstructions for ENSO phenomena (El-Nina and La-Nina) and IOD phenomena (positive IOD and negative IOD) in the ASO and NDJ seasons are displayed in Figures 13–14. The majority of Indonesia experiences a rainfall deficit during the ASO season with good IOD events. In the southern section of Sumatra, Java, and southern Kalimantan, which receives more rainfall than other locations, the rainfall season begins during the NDJ season. Interestingly, nevertheless, the northern region of Sumatra has a comparatively high surplus of rainfall in positive IOD years rather than a deficit during peak positive IOD event (ASO) years. A distinct pattern can be seen in the combined rainfall anomaly during negative IOD episodes.

The majority of Indonesia's land encompassed by the EOF1, EOF2, and EOF3 sectors faces a rainfall deficit during the ASO dry season. The EOF2 region isn't any worse than the other two zones, though. Particularly when both El Nino and Positive IOD occurrences happen, and it is even worse when they

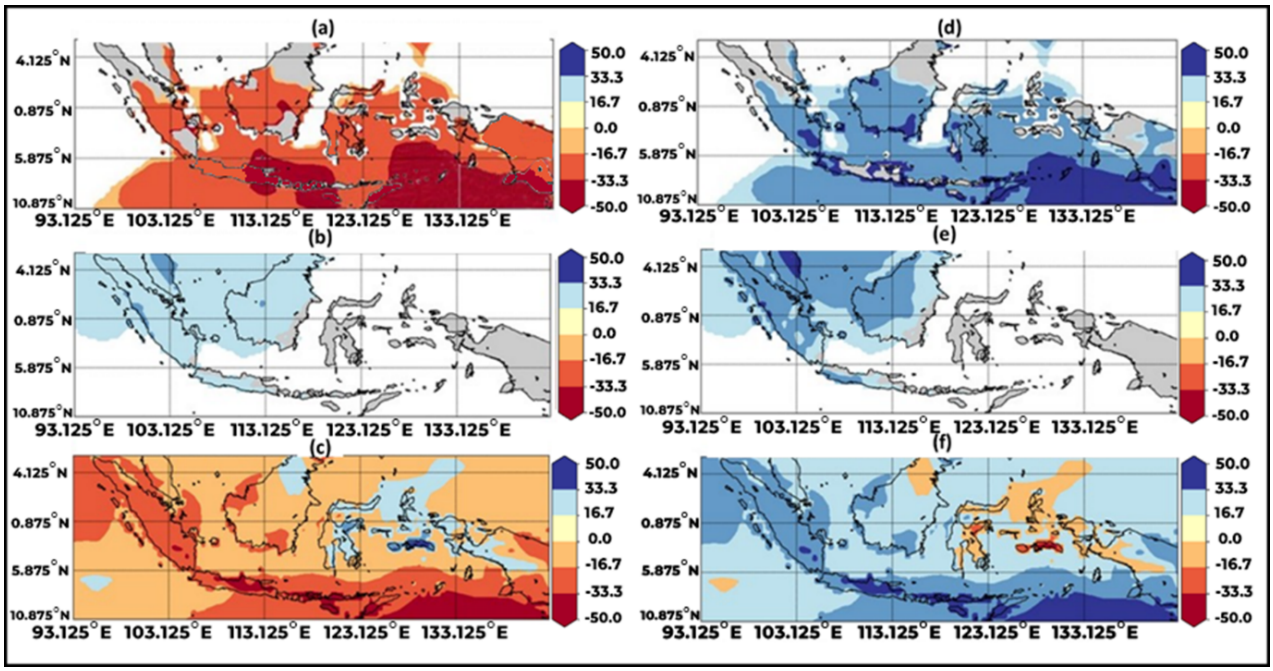

Figure 13. Composite EOF during El Nino and La Nina Seasons for the ASO (left) and NDJ (right): (a) (d) EOF1, (b) (e) EOF2, and (c) (f) EOF3. The Two-Tailed t-Test's 95% Significant Rainfall Anomalies Are Indicated by Color

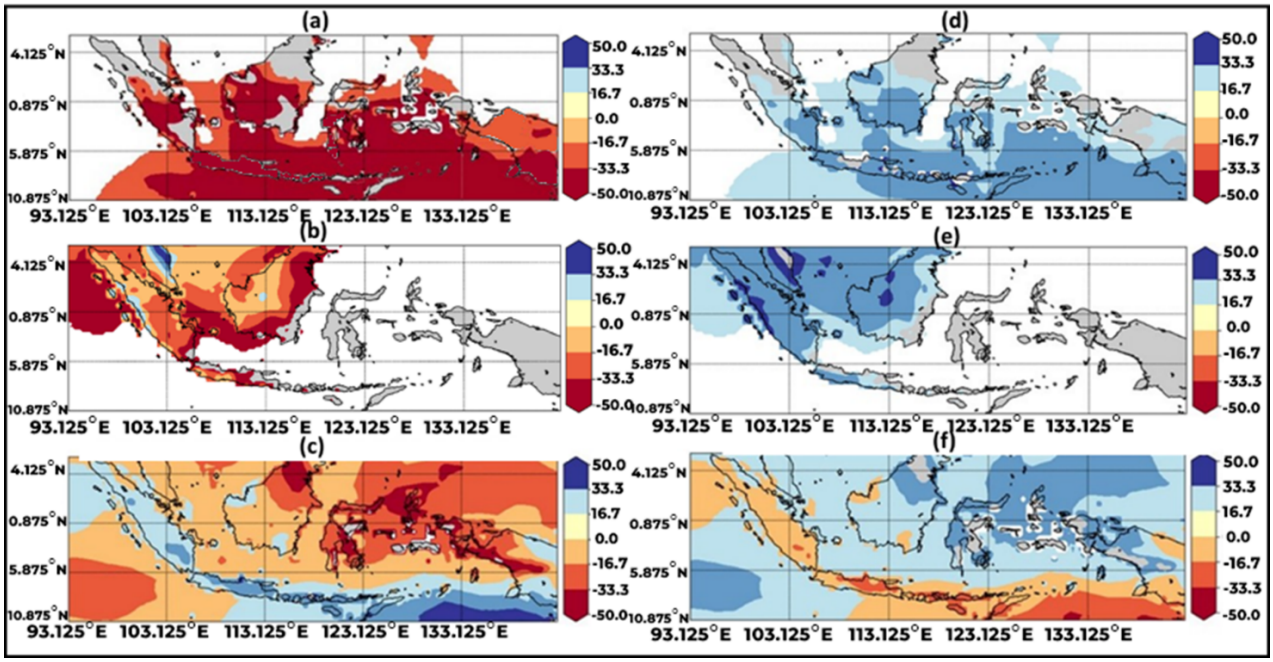

Figure 14. Composite EOF throughout Positive IOD and Negative IOD Seasons for ASO (left) and NDJ (right): (a) (d) EOF1, (b) (e) EOF2, and (c) (f) EOF3 for the ASO (left) and NDJ (right) Seasons. The Two-tailed t-test's 95% Significant Rainfall Anomalies Are Indicated by Color

do so together. El Nino composite rainfall anomalies exhibit a pattern resembling positive IOD events. Though it affects a larger area, drought (negative rainfall anomaly) during El Nino events, particularly in the ASO season, is not as severe as it is during positive IOD occurrences. Conversely, when La Nina is practically certain, there is an excess of rainfall during the ASO season in every part of Indonesia, with the exception of the.

During the NDJ wet season, all major EOF mode regions mostly show a rainfall surplus (composite results not shown), especially the EOF1 and REOF2 regions, with the EOF2 region being much higher and positive than the other two regions. The excess rainfall in the NDJ wet season is mostly caused by La Nina and Negative IOD years, and it gets worse when they happen at the same time. The differences in rainfall that occur in all EOF reconstruction modes during the ENSO and IOD phenomena years are clearly illustrated. These two phenomena have a big impact on the climate in Indonesia.

Researchers studying climate change find it crucial to identify Indonesia's climatic type based on rainfall characteristics and current data. Based on EOF statistics, this study has assessed and observed the extent to which the ENSO and IOD phenomena impact Indonesia's climate. As a result, it is crucial for the general public to be aware of the temporal and spatial distribution of rainfall in Indonesia, particularly the government, which sets policies. This research helps paint a clear picture of the potential effects of the dynamics of the Tropical Indian Ocean (TIO) and Tropical Pacific Ocean (TPO) during a climate mode anomaly on Indonesia's climate change. The greatest risks to the social and economic well-being of a society are hydrometeorological disasters, which policymakers can mitigate by adopting the appropriate attitude

4. CONCLUSIONS

This study clearly shows that there is a monsoon season in Indonesia based on Indonesia's main rainfall patterns. We can determine the temporal and geographical patterns of seasonal rainfall using the EOF technique. These simulations' results unquestionably show that the Indonesian region suffers an abundance of patterns of rainfall variability. The first PC explained 38.57% of the total rainfall variance in Indonesia, the second PC 13.92%, and the third PC 8.93%. Rainfall in Indonesia fluctuates widely. The first dominating PC variance explains less than half of the overall variance. At the peak of the dry season (ASO), there is a significant correlation (> 0.85) between the predominant rainfall pattern in Indonesia and SST and wind, which decreases at the initial phase of the rainy season (NDJ). The predominant pattern of rainfall clearly indicates that the dry season, which runs from May to October, is marked by strong easterly winds and a notable drop in precipitation. November through April is when the rainy season occurs. The present study offers conclusive responses to the inquiries posed by the scientific community on the presence of monsoon and regional precipitation in Indonesia. The variability of Indonesia's dominant rainfall is studied by correlating Indonesia's dominant rainfall with local SST. This variability definitively shows that rising local SST causes increasing and sensitivity to changes in rainfall in Indonesia.

5. ACKNOWLEDGMENT

The authors thank the anonymous reviewer for the constructive comments and suggestions. The anonymous reviewer's insightful remarks and recommendations are much appreciated by the authors. The Ministry of Education, Culture, Research, and Technology has supported this study as part of the first author's dissertation under Doctoral Dissertation Research Grant 2024, No. 0667/E5/AL.04/2024.

REFERENCES

Aldrian, E. and D. Susanto (2003). Identification of Three Dominant Rainfall Regions within Indonesia and Their Relationship to Sea Surface Temperature. *International Journal of Climatology*, **23**(12); 1435–1452

Annamalai, H., S. Kida, and J. Hafner (2010). Potential Impact of the Tropical Indian Ocean-Indonesian Seas on El Nino Characteristics. *Journal of Climate*, **23**(14); 3933–3952

Ariska, M., M. Irfan, and I. Iskandar (2024a). Spatio-Temporal Variations of Indonesian Rainfall and Their Links to Indo-Pacific Modes. *Atmosphere*, **15**(1036); 1–18

Ariska, M., S. Suhadi, S. Supari, M. Irfan, and I. Iskandar (2024b). Annual and Interannual Rainfall Variability in Indonesia Using Empirical Orthogonal Function (EOF) Analysis and Its Response to Ocean-Atmosphere Dynamics. *Physical Sciences Journal*, **16**(2); 151–165

Baeda, A. Y., C. Pao'Tonan, and D. Abdullah (2019). The Correlation between Sea Surface Temperature and MJO Incidence in Indonesian Waters. *IOP Conference Series: Earth and Environmental Science*, **235**(1); 012020

Beck, H. E., N. Vergopolan, M. Pan, V. Levizzani, A. I. Van Dijk, G. P. Weedon, L. Brocca, F. Pappenberger, G. J. Huffman, and E. F. Wood (2017). Global-scale evaluation of 22 precipitation datasets using gauge observations and hydrological modeling. *Hydrology and Earth System Sciences*, **21**(12); 6201–6217

Campos, C., F. T. Couto, F. L. M. Santos, J. Rio, T. Ferreira, and R. Salgado (2024). ECMWF Lightning Forecast in Mainland Portugal During Four Fire Seasons. *Atmosphere*, **15**(2); 156

Chang, C. P., Z. Wang, J. Ju, and T. Li (2004). On the Relationship between Western Maritime Continent Monsoon Rainfall and ENSO During Northern Winter. *Journal of Climate*, **17**(3); 665–672

Chang, C. P., W. Zhuo, M. John, and L. Ching-Hwang (2005). Annual Cycle of Southeast Asia — Maritime Continent Rainfall and the Asymmetric. *Journal of Climate*, **18**; 287–301

Cooley, J. W., P. A. W. Lewis, and P. D. Welch (1969). The Fast Fourier Transform and Its Applications. *IEEE Transactions on Education*, **12**(1); 27–34

Estrela, M. J., D. Corell, J. J. Miró, and R. Niclós (2024). Analysis of Precipitation and Drought in the Main Southeastern Iberian River Headwaters (1952–2021). *Atmosphere*, **15**(2); 166

Fukuoka, A. (1951). A study of 10-day forecast (a synthetic report). *Geophys. Mag.*, **22**; 177–218

Ge, J., X. Jia, and H. Ma (2024). Pacific Decadal Oscillation Modulation on the Relationship between Moderate El Niño-

Southern Oscillation and East Asian Winter Temperature. *Atmosphere*, **15**(2)

Hendon, H. H. (2003). Indonesian Rainfall Variability: Impacts Of ENSO and Local Air-Sea Interaction. *Journal of Climate*, **16**(11); 1775–1790

Horii, T., E. Siswanto, I. Iskandar, I. Ueki, and K. Ando (2022). Can Coastal Upwelling Trigger a Climate Mode? A Study on Intraseasonal-Scale Coastal Upwelling off Java and the Indian Ocean Dipole. *Geophysical Research Letters*, **49**(15); 1–9

Igarashi, T. and D. Suryadarma (2023). Foundational Mathematics and Reading Skills of Filipino Students Over a Generation. *International Journal of Educational Development*, **96**; 102688

Iskandar, I., D. O. Lestari, A. D. Saputra, R. Y. Setiawan, A. Wirasatriya, R. D. Susanto, W. Mardiansyah, M. Irfan, Rozirwan, J. D. Setiawan, and Kunarso (2022). Extreme Positive Indian Ocean Dipole in 2019 and Its Impact on Indonesia. *Sustainability (Switzerland)*, **14**(22); 1–15

Iskandar, I., Q. W. Sari, D. Setiabudidaya, I. Yustian, and B. Monger (2017). The Distribution and Variability of Chlorophyll-A Bloom in the Southeastern Tropical Indian Ocean Using Empirical Orthogonal Function Analysis. *Biodiversitas*, **18**(4); 1546–1555

Iskandar, I., T. Tozuka, Y. Masumoto, and T. Yamagata (2008). Impact of Indian Ocean Dipole on Intraseasonal Zonal Currents at 90°e on the Equator As Revealed by Self-Organizing Map. *Geophysical Research Letters*, **35**(14); 1–5

Kajita, R., M. D. Yamanaka, and O. Kozan (2022). Reconstruction of Rainfall Records at 24 Observation Stations in Sumatera, Colonial Indonesia, from 1879–1900. *Journal of Hydrometeorology*, **23**(10); 1–71

Katsumata, M., S. Mori, J.-I. Hamada, M. Hattori, F. Syamsudin, and M. D. Yamanaka (2018). Diurnal cycle over a coastal area of the Maritime Continent as derived by special networked soundings over Jakarta during HARIMAU2010. *Progress in Earth and Planetary Science*, **5**(1); 6

Kurniawati, N., D. O. Lestari, Fauziyah, D. Setiabudidaya, and I. Iskandar (2020). Variation of Thermodynamic Layers Over the South Coastal Java Region (sjcr) and Their Influences on Nutrient Abundance. *Journal of Physics: Conference Series*, **1568**(1)

Lestari, D. O., E. Sutriyono, S. Kadir, and I. Iskandar (2019). Impact of 2016 Weak La Nina Modoki Event Over the Indonesian Region. *International Journal of GEOMATE*, **17**(61); 156–162

Liu, J., L. Zhao, J. Wang, and Z. Xiao (2024). Detecting Relationship between the North–South Difference in Extreme Precipitation and Solar Cycle in China. *Atmosphere*, **15**(2); 175

Lorenz, E. N. (1956). Empirical orthogonal functions and statistical weather prediction. Technical Report Statistical Forecast Project Rep. 1

Lyons, W. (1982). Empirical Orthogonal Function Analysis of Hawaiian Rainfall. *Journal of Applied Meteorology*, **21**; 1713

Mulsandi, A., Y. Koesmaryono, R. Hidayat, A. Faqih, and A. Sopaheluwakan (2024). Detecting Indonesian Monsoon Signals and Related Features Using Space–Time Singular Value Decomposition (SVD). *Atmosphere*, **15**(2); 1–15

Nugroho, A. R., I. Tamagawa, and M. Harada (2021). The Relationship etween River Flow Regimes and Climate Indices of ENSO and IOD On Code River, Southern Indonesia. *Water (Switzerland)*, **13**(10); 1–14

Obukhov, A. (1947). Statistically homogeneous fields on a sphere. *Usp. Mat. Nauk*, **2**; 196–198

Obukhov, A. (1960). The statistically orthogonal expansion of empirical functions. *Bull. Acad. Sci. USSR, Geophys. Ser.*, **1**; 288–291

Tang, Q., Y. Zhao, Y. He, Q. Yu, and T. Liang (2024). Analysis of Aerosol Types and Vertical Distribution in Seven Typical Cities in East Asia. *Atmosphere*, **15**(2); 195

Yamanaka, M. D. (2016). Physical Climatology of Indonesian Maritime Continent: An Outline to Comprehend Observational Studies. *Atmospheric Research*, **178–179**; 231–259

Yamanaka, M. D. (2018). Equatorial Rainfall and Global Climate. *ISQUAR*, **3**; 3–6

Zhang, Q., Q. Tang, X. Liu, S. M. Hosseini-Moghari, and P. Attarod (2020). Improving Princeton Forcing Dataset Over Iran Using the Delta-Ratio Method. *Water (Switzerland)*, **12**(3); 1–15

Zheng, X.-T. (2019). Indo-Pacific Climate Modes in Warming Climate: Consensus and Uncertainty across Model Projections. *Current Climate Change Reports*, **5**(4); 308–321